Journal of Materials Chemistry A

ROYAL SOCIETY OF CHEMISTRY

PAPER

View Article Online
View Journal | View Issue

Cite this: J. Mater. Chem. A, 2025, 13, 35316

Does the presence of CO_2 affect the alkaline stability of anion-exchange membranes?

Sapir Willdorf-Cohen,[a] Songlin Li,[a] Simcha Srebnik,[b] Charles E. Diesendruck *[cd] and Dario R. Dekel *[ade]

Anion-exchange membranes (AEMs) enable electrochemical energy devices to operate in alkaline environments, allowing the use of earth-abundant, platinum group metal-free catalysts. This makes them highly attractive for applications such as AEM fuel cells (AEMFCs), water electrolyzers (AEMWEs), and oxygen separators (AEMOSs). However, two key challenges still hinder their commercialization: chemical degradation of the membranes and carbonation from atmospheric CO_2, both of which impair conductivity and reduce long-term performance. Building upon our *ex situ* novel technique to measure the alkaline stability of quaternary ammonium salts (QAs) and AEMs at different hydroxide hydration levels, in this study we investigate the effect of CO_2 on the stability of the AEMs. Specifically, we evaluate the stability of AEM standard benzyltrimethyl ammonium cations ($BTMA^+$) in the presence of mixtures of hydroxide and (bi)carbonate anions at different ratios and hydration levels. Additionally, we introduce a novel technique to simultaneously evaluate (bi)carbonate impact and hydroxide conductivity in AEMs. Our results reveal that the presence of (bi)carbonate anions surrounding $BTMA^+$ significantly reduces QA degradation. This phenomenon is further supported by molecular dynamics simulations, which suggest a "salting-out" effect, where water more strongly hydrates hydroxide ions, isolating them from the organic QA sites and reducing degradation probability. These findings provide new insight into AEM behavior in CO_2-containing environments such as ambient air. This study provides new, valuable data to overcome the critical challenge of AEM alkaline stability and opens new avenues for the design of more durable AEM materials, advancing the development of AEMFCs, AEMWEs, and AEMOSs for real-world applications.

Received 29th July 2025
Accepted 15th September 2025

DOI: 10.1039/d5ta06137g

rsc.li/materials-a

1. Introduction

Anion-exchange membrane (AEM) fuel cells (AEMFCs) and anion-exchange membrane water electrolyzers (AEMWEs) have been attracting significant attention as promising green and efficient technologies for energy conversion and storage. Recently, novel anion-exchange membrane oxygen separators (AEMOSs) were also developed. All these electrochemical technologies operate in an alkaline environment, and thus, allow the use of precious metal-free and critical raw material-free electrocatalysts from a wide selection of affordable and abundant materials, as well as fluorinated-free, low-cost anion-exchange membranes (AEMs).[1–12] Despite the significant progress recently achieved in AEM-based electrochemical research, the commercial development is primarily impeded by:[1] degradation processes in AEMs during the cell operation, and[2] carbonation processes in AEMFCs and water-fed dry-cathode AEMWEs.[3,13–18]

The chemical decomposition of the AEMs during cell operation remains the main concern and challenge, limiting the operation time of these technologies.[19–24] The combination of a high alkaline environment and high operating current densities in the AEMFC and dry-cathode AEMWE results in low hydration of the cathodes and AEM/cathode interface (Fig. 1).[25–28] In these conditions, the generated hydroxide anions have limited water microsolvation, turning them into extremely reactive nucleophiles and bases.[26,29–31] This, in turn, accelerates the degradation at the AEM/cathode interface,[28,32,33] leading to a detrimental reduction in anion conductivity and therefore in *operando* cell performance over time.[34–37]

In order to overcome the stability issues of AEMs, significant efforts have been made mainly in the synthesis of highly alkaline-stable quaternary ammonium (QA),[21,27,33,38–55] sulfonium and phosphonium salts,[56–59] as well as metal ions,[60–65] as

[a]The Wolfson Department of Chemical Engineering, Technion – Israel Institute of Technology, Haifa 3200003, Israel. E-mail: dario@technion.ac.il
[b]Department of Chemical and Biological Engineering, University of British Columbia, Vancouver, Canada
[c]Schulich Faculty of Chemistry, Technion – Israel Institute of Technology, Haifa 3200003, Israel. E-mail: charles@technion.ac.il
[d]The Nancy & Stephen Grand Technion Energy Program (GTEP), Technion – Israel Institute of Technology, Haifa 3200003, Israel
[e]Israel National Institute of Energy Storage (INIES), Technion – Israel Institute of Technology, Haifa 3200003, Israel

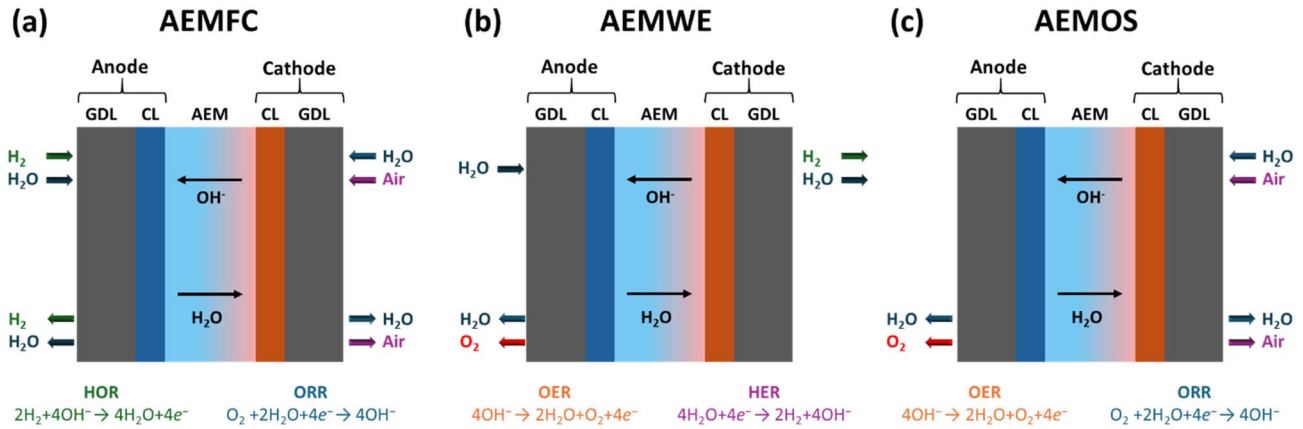

Fig. 1 Schematic diagram showing hydration level (high hydration areas in blue and low hydration areas in red), direction of the migration of OH^- anions and diffusion of water, and electrochemical reactions at the electrodes during operation in (a) AEMFC, (b) AEMWE in dry cathode operation mode, and (c) AEMOS devices.

cationic functional groups for AEMs. In addition, new adequate techniques for predicting the chemical stability of AEMs in *ex situ* tests that mimic real cell operation conditions have also been developed.[28,66–70]

Conventional tests to measure the alkali *ex situ* stability consist of the immersion of cationic model molecules and polymers in a basic aqueous solution at different concentrations (1–10 M KOH) and temperatures (from room temperature up to 160 °C).[19,38,47,71] However, these tests do not adequately simulate the conditions found in *operando* cells, because even at a high concentration of 10 M KOH aqueous solution, the hydroxide hydration level is significantly higher than the one found around the cathode electrode in the operating cell.[25,32,72]

One of the newly emerged *ex situ* techniques is our recently developed technique to measure the alkaline stability of AEMs. This method simulates the *operando* environment of AEMs in high-current electrochemical devices.[28,69] It relies on generating mobile anhydrous hydroxide anions (OH^-) by oxidizing potassium (K) metal *in situ*, then forming a complex of K^+ with 18-crown-6 ether (CE), resulting in CE-K^+/OH^- in water-free DMSO-d_6. Using this protocol, we have studied the stability of numerous QA cations and AEM polymers dissolved in non-aqueous solvents, mimicking the low hydration environment of AEMFC and AEMWE cathodes and AEM/cathode interface. Using this technique, we consistently found that all AEM cationic species degrade very rapidly at low hydration levels λ, particularly when there are four or fewer water molecules per hydroxide anion ($\lambda \leq 4$) available for solvation.[28] However, when the number of water molecules per hydroxide anion reaches or exceeds five ($\lambda \geq 5$), the OH^- first solvation sphere is full, and the anion becomes significantly less nucleophilic and basic, and thus the alkali degradation of the AEM polymer is reduced.[29]

Besides the important effect of low hydration on the stability, several studies have shown that the presence of CO_2 is critical and must be considered in the development of practical AEMFC and AEMWE systems.[13,14,18,73–76] Therefore, whenever ambient air (which contains ~400 ppm of carbon dioxide) is involved (both as a feed in AEMFCs or equilibrium with water feed in AEMWEs), AEMs face a critical technological challenge – the so-called carbonation process.[76,77] While alkaline stability is typically tested under very controlled conditions,[28,69,70] in reality, the carbonation process is scarcely considered in such tests. In the carbonation process, the CO_2 dissolves in water and reacts with the hydroxide anions in the cell, to form (bi)carbonate anions according to the following equations:

$$OH^- + CO_2 \rightleftharpoons HCO_3^- \quad (1)$$

$$HCO_3^- + OH^- \rightleftharpoons CO_3^{2-} + H_2O \quad (2)$$

In AEMWEs, performance is enhanced by employing a supportive hydroxide or carbonate ion electrolyte, improving conductivity and activating the electrocatalyst. However, challenges arise from water transfer, membrane degradation, and electrolyte carbonation.[78,79] The carbonation process occurring in the AEM and supporting electrolyte reduces the mobility of carbonate species, leading to increased ohmic resistance. Additionally, carbonation of the ionomer lowers the local pH, resulting in decreased catalytic efficiency.[80] In general, the formation of (bi)carbonates due to the presence of CO_2 in the ambient air reduces the conductivity of the AEM and, therefore, the cell performance as well.[77] In the case of AEMFCs, researchers have gained insight into the impact of CO_2 on cell performance through a range of recent experimental studies and modeling efforts.[14,76,81–83] The majority of these studies focus on determining the conditions required to mitigate the carbonate reaction and reduce the amount of the three carbon-containing species in the membrane, CO_2, HCO_3^-, and CO_3^{2-}.

More recent studies propose various approaches to reduce the voltage penalty caused by CO_2 in AEMFCs. These include increasing current density, raising cell temperature and hydration level, and decreasing cathode flow rate.[82–84] A recent numerical model of ambient air-fed AEMFC showed that operating at higher current densities has two benefits. Firstly, it enhances the general performance and the power densities of

the cell, even though an expected decrease in AEM performance at high current densities (generally above 1000 mA cm^{-2}) is anticipated.[13,32] Secondly, it enables the reduction of the impact of CO_2 on the cell performance, as at higher current densities the (bi)carbonate concentration in the cell is negligible, allowing for effective operation with ambient air.[76]

All the previously mentioned studies focused on the effect of CO_2 on cell performance; however, to the best of our knowledge, no one has considered whether the presence of CO_2 affects the stability of the AEM and, therefore, the electrochemical cell. In a pioneering work in this direction, Srebnik & Dekel investigated the influence of carbonate anions on the alkaline stability of benzyl trimethylammonium-based QA compounds ($BTMA^+$) through Molecular Dynamics (MD) simulations. Their study reveals that carbonate anions display a greater affinity for water than hydroxides and therefore are more hydrated.[85] Consequently, due to the presence of carbonate anions, the hydroxide anions have less water to solvate, which in turn makes them more reactive towards the QA cations. This, in turn, increases the degradation of the QA.[31] This effect is reported to be more pronounced at low hydration levels. On the other hand, it was also reported that the carbonate anions concentrate sufficiently near $BTMA^+$. As a result, the access of hydroxides to the $BTMA^+$ is diminished compared with the carbonate-free scenario, thereby stabilizing the QA. Thus, it was concluded that the impact of carbonate anions protecting the $BTMA^+$ *versus* the improved reactivity of unsolvated hydroxide anions required further investigation.[85]

To thoroughly investigate the effect of (bi)carbonates on the alkaline stability of QAs, in this study we developed a new experimental protocol to determine the effect of the carbonation process on the hydroxide-induced $BTMA^+$ degradation, specifically at low hydration levels. To the best of our knowledge, this is the first study that experimentally investigates the effect of CO_2 on AEM stability, with support from MD simulations.

2. Methods section

2.1 Experimental section

2.1.1 Materials. CE-K^+/OH^- complex was prepared as described previously,[28,29] stored, and handled in a glovebox (water and O_2 kept at <1 ppm levels). Nuclear magnetic resonance (NMR) tubes (Wilmad-LabGlass) with septum were used for kinetic studies. BTMA, in its bromide form, was purchased from Sigma-Aldrich. Commercial FAA-3-30 AEM with 30 μm dry thickness was obtained from Fumatech® (IEC = 1.5–1.8 mmol gr^{-1}). All other materials, unless otherwise stated, were used without additional purification.

2.1.2 Preparation of water-free hydroxide and (bi) carbonate solutions. In a glovebox, a CE-K^+/OH^- solution was prepared by weighing 0.5 mmol from the CE-K^+/OH^- complex and dissolving it in anhydrous DMSO-d_6 following the procedure developed in ref. 28. The solution was then divided according to the targeted hydroxide-(bi)carbonate ratio in the specific experiment. Part of the solution was separated to be used as the hydroxide ion solution (solution 1), and the remaining solution was transferred into a Schlenk glass tube to undergo conversion into a (bi)carbonate solution. The Schlenk was sealed with a septum and insulating tape and removed from the glove box. CO_2 gas (99.99999%) was bubbled into this solution to react with the hydroxide anions, resulting in the formation of dry (bi)carbonate in DMSO-d_6, (solution 2). This is a complete reaction as under alkaline conditions, dissolved CO_2 reacts rapidly with OH^- to form bicarbonate (eqn (1)), and at high pH, further equilibrates to carbonate (eqn (2)). These well-established reactions confirm that the interaction of OH^- with CO_2 indeed yields (bi)carbonate species.[86] Finally, the Schlenk with solution 2 was returned to the glove box.

2.1.3 Kinetic studies of $BTMA^+$ alkaline degradation. In order to understand the effect of the carbonation on the stability of the BTMA+, *ex situ* stability tests were conducted utilizing varying concentrations of hydroxides and (bi)carbonates. The concentration of these anions within a 0.5 ml of DMSO-d_6, were calculated by:

$$[\text{(Bi)carbonate }]_M = \frac{[\text{(bi)carbonate }]_{mmol}}{0.5\ ml} \quad (3)$$

$$[OH^-]_M = \frac{[OH^-]_{mmol}}{0.5\ ml} \quad (4)$$

All test conditions are summarized in Tables 1 and S1. Hence, we also defined the effective hydration number of the solution, λ effective (λ_{eff}), as follows:

$$\lambda_{(eff)} = \frac{[H_2O]_{mmol}}{[OH^- + \text{(bi)carbonate}]_{mmol}} \quad (5)$$

This initial set of experiments was carried out at low hydration levels, specifically with $\lambda_{eff} = 1$ and 4 (Fig. S2). In further experiments, the hydroxide concentration was consistently maintained at fixed levels (0.9 M and 0.7 M) while the (bi) carbonate concentration was varied. For 0.9 M OH^- the (bi) carbonate concentration was 0, 0.05, and 0.1 M (Tables S2 and S3); and for 0.7 M OH^- (bi)carbonate concentration was 0, 0.15, and 0.3 M (Tables 2 and S4). For each OH^- concentration, we conducted tests at two distinct hydration levels. Here, we defined λ_{OH^-} as:

$$\lambda_{OH^-} = \frac{[H_2O]_{mmol}}{[OH^-]_{mmol}} \quad (6)$$

Consistently, with an OH^- concentration of 0.9 M, the corresponding calculated λ_{OH^-} values are 1.1 and 4.4. The experiments with $\lambda_{OH^-} = 1.1$ and 4.4 were repeated three times from independent preparations (Fig. S2) to determine the sample standard deviation of measurements. Similarly, when employing a 0.7 M OH^- concentration, the calculated $\lambda_{OH^-} =$ values are 1.4 and 5.7. To be able to describe the solvation state of the (bi) carbonate, in addition to the hydroxide, we also defined $\lambda_{(bi)carbonate}$ as:

$$\lambda_{(bi)carbonate} = \frac{[H_2O]_{mmol}}{[\text{(bi)carbonate}]_{mmol}} \quad (7)$$

Table 1 Degradation rates and calculated half-lives for $BTMA^+$ with 0, 0.1, 0.3, 0.5, and 1 M (bi)carbonates in DMSO-d_6 solutions at 45 °C with λ_{eff} = 1 and 4

	λ_{eff}							
	$\lambda_{eff} = 1$				$\lambda_{eff} = 4$			
(Bi)carbonate [M]	λ_{OH^-}	$\lambda_{(bi)carbonate}$	Rate constant [h^{-1}]	Calculated half-life $t_{1/2}$ [h]	λ_{OH^-}	$\lambda_{(bi)carbonate}$	Rate constant [h^{-1}]	Calculated half-life $t_{1/2}$ [h]
0	1	0	6.62×10^{-2}	10.5	4	0	1.96×10^{-3}	353
0.1	1.1	10	4.82×10^{-2}	14.4	4.4	40	1.25×10^{-3}	554
0.3	1.4	3.3	1.35×10^{-2}	51.3	5.7	13.3	6.35×10^{-4}	1090
0.5	2	2	1.12×10^{-2}	61.9	8	8	1.22×10^{-4}	5672
1	0	1	2.41×10^{-8}	$>1 \times 10^6$	0	4	6.21×10^{-10}	$>1 \times 10^6$

For each experiment, three DMSO-d_6 solutions were prepared inside a glovebox with a dry N_2 atmosphere: solutions 1–3. The NMR tube was filled with the calculated ratio of solutions 1 and 2 and with additional DMSO-d_6 (Tables S1, S2, and S4). The tube was double-sealed with Teflon tape and a septum to avoid any potential contamination. Solution 3, which contained the dissolved QA in anhydrous DMSO-d6, was transferred to a 1 ml disposable syringe sealed with parafilm and removed from the glovebox along with the NMR tube. Before initiating the experiment, precise quantities of ultra-pure water (UPW) were inserted into the NMR tube to change the microsolvation state of the anions until the desired λ is achieved. Subsequently, solution 3 was added. The NMR tube was immediately introduced into the instrument to start the $BTMA^+$ concentration measurements. NMR spectra were recorded in a Bruker AVANCE III 400 MHz or Bruker AVANCE 300 MHz spectrometer. The chemical shifts are referenced to signal at $\delta = 0.00$ (TMS) or partially undeuterated solvent peaks. The relevant aromatic signals were integrated over time to measure the reaction progress. All stability tests were conducted at 45 °C. Representative calculations for eqn (3)–(7) and concentrations are included in the SI.

2.1.4 Anion conductivity and *ex situ* AEM stability measurements. The AEM samples were first converted into their HCO_3^- form by immersing them in 1 M $KHCO_3$. Then, the samples were placed in a membrane testing system (MTS 740, Scribner Associates Inc.) to perform stability tests in three different forms: OH^-, HCO_3^-, and in mixed form (OH^-/HCO_3^-). The procedure to obtain the true OH^- conductivity of an AEM was done following the protocol previously described by Dekel *et al.*[87,88] The membrane in bicarbonate form underwent decarbonation through *in situ* exchange with hydroxide anions. This exchange occurred by splitting water using a direct current (generated by Ivium-*n*-Stat, Ivium Technologies) of 0.1 mA through two platinum mesh electrodes. All experiments were conducted under an N_2 flow rate of 500 sccm at 80 °C and a relative humidity (RH) of 60% on the AEM. This enables the decarbonation process to take place until the HCO_3^- and CO_3^{2-} anions are completely displaced by OH^- anions. Once the true OH^- conductivity is reached, the alkali stability of the AEM was determined by the decay of OH^- conductivity over time.[58,66] The mixed OH^-/HCO_3^- form in the AEM was achieved by stopping the applied direct current at the midpoint of the highest true OH^- conductivity. The membrane stability was then similarly measured by the reduction in anion conductivity over time. The stability of the AEM in its bicarbonate form was measured without applying the current to ensure no hydroxide ions are formed, and then keeping the HCO_3^- in the AEM during the stability test.

2.2 Computational methods

All-atom MD simulations of $BTMA^+$ in DMSO were carried out using the LAMMPS software package.[89] Water was modeled as rigid molecules using the SPC/E potential,[90] carbonate anions were modeled using the CHARMM force field,[91] and $BTMA^+$, hydroxide, and carbonate anions were modeled using the OPLS force field.[92] A cutoff distance of 10 Å was used for non-bonded

Table 2 Degradation rates and calculated half-lives for $BTMA^+$ at 0, 0.15, and 0.3 M (bi)carbonates in DMSO-d_6 solutions at 45 °C at a fixed initial OH^- concentration of 0.7 M with λ_{OH^-} = 1.4 and 5.7

	0.7 M OH^-			
	$\lambda_{OH^-} = 1.4$		$\lambda_{OH^-} = 5.7$	
(Bi)carbonate [M]	Rate constant [h^{-1}]	Calculated half-life $t_{1/2}$ [h]	Rate constant [h^{-1}]	Calculated half-life $t_{1/2}$ [h]
0	4.02×10^{-2}	17.2	9.59×10^{-4}	723
0.15	2.18×10^{-2}	31.8	5.39×10^{-4}	1286
0.3	1.16×10^{-2}	59.8	4.82×10^{-4}	1438

interactions and the simulation time step was set to 1 fs. The concentration of carbonate anions was varied in the range of 0–0.1 M. Water/hydroxide molar ratios of 1.4 and 5.7 were considered, and a 10 : 1 hydroxide : $BTMA^+$ was used for all simulations, consistent with the experimental set-up. The system was kept in charge neutral by adding the appropriate number of potassium cations or bromine anions and DMSO, the latter used as a solvent. Periodic boundaries were imposed, and the system was equilibrated using the isothermal-isobaric ensemble (NPT) for 200 ps at 298 K and 1 atm. The resulting cubic simulation box was approximately 4.2 nm in length after equilibration. Thirty heating and cooling cycles were used for the production stage. Each cycle consisted of 4 steps:[1] 100 ps canonical ensemble (NVT) heating to 600 K,[2] 300 ps NVT cooling to 298 K,[3] 100 ps NPT equilibration, and[4] 100 ps data collection every 1 ps under NVT ensemble conditions. Nosé-Hoover thermostat and barostat were used with temperature and pressure dampening parameters of 100 fs and 1000 fs, respectively.[93]

3. Results and discussion

We investigated the effect of carbonation on the stability of $BTMA^+$ at low hydration levels of $\lambda_{eff} = 1$ and 4. It is known that $BTMA^+$ typically undergoes a S_N2 reaction with hydroxide, as illustrated in Fig. 2a.[94,95] The kinetics of this reaction was determined by analyzing the changes in the aromatic region of the QA (7.5–7.6 ppm) and its degradation product peak (7.0–7.2 ppm) using ^{1}H-NMR integration (Fig. S3–S14 and Tables S5–S16).[31]

Fig. 2b shows $BTMA^+$ stability results under different concentrations of (bi)carbonate: 0 (pure OH^-), 0.1, 0.3, 0.5, and 1 M (pure (bi)carbonate)) for $\lambda_{eff} = 1$ and 4. As can be seen in Fig. 1b ($\lambda_{eff} = 1$), $BTMA^+$ rapidly degrades when the solution contains only hydroxide anions (0 M). The calculated half-life of $BTMA^+$ under these conditions was determined to be 10.5 h (Table 1). The high degradation rate is due to the low hydration of the solution, consistent with our previous results.[28,29] When (bi)carbonate anions are added, the $BTMA^+$ degrades more slowly. The calculated half-lives of $BTMA^+$ were found to be 14.4, 51.3, and 61.9 h, for 0.1, 0.3, and 0.5 M (bi)carbonates, respectively (Fig. 2b and Table 1). When the solution contains only (bi) carbonates (1 M), no degradation of the $BTMA^+$ was detected after 12 h of stability test. These results demonstrate a clear trend in which, at constant $\lambda_{eff} = 1$, $BTMA^+$ cations degrade more slowly as the concentration of (bi)carbonate increases. This means that in an *operando* AEMFC, while keeping the same hydration in the membrane, carrying the charge with increasing (bi)carbonates (instead of hydroxide), may reduce the AEM anion conductivity, affecting the cell performance, but this in turn will increase the AEM stability and therefore, the AEMFC performance stability.

Fig. 2c presents the results of $BTMA^+$ stability tests at $\lambda_{eff} = 4$, utilizing the same concentrations of (bi)carbonates. As can be seen in Fig. 2c, the half-lives of $BTMA^+$ were considerably longer at $\lambda_{eff} = 4$. The calculated $BTMA^+$ half-lives for 0, 0.1, 0.3, and 0.5 M (bi)carbonate were determined to be 353, 554, 1090, and 5672 h, respectively. In addition, when only (bi)carbonate is present, again, $BTMA^+$ remains undegraded. These results are consistent with the trend observed at lower hydration levels, demonstrating that higher concentrations of (bi)carbonates contribute to increasing the stability of the $BTMA^+$ in alkaline media.

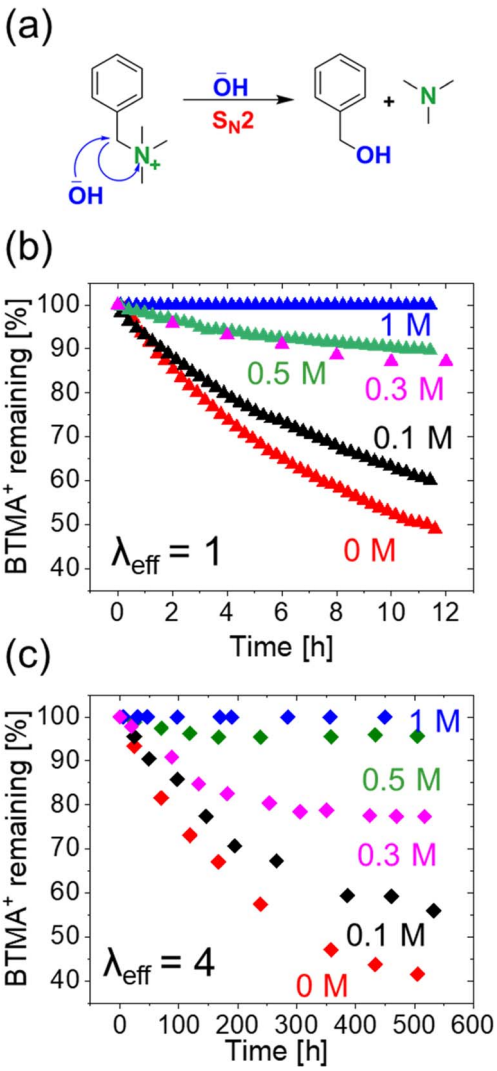

Fig. 2 (a) Degradation mechanism of $BTMA^+$ with OH^- by nucleophilic attack (S_N2). Relative $BTMA^+$ remaining as a function of time in DMSO-d_6 solutions at 45 °C with 0, 0.1, 0.3, 0.5, and 1 M (bi)carbonates for: (b) $\lambda_{eff} = 1$, and (c) $\lambda_{eff} = 4$.

Fig. 2c further demonstrates the slower degradation rate of $BTMA^+$ under higher hydration conditions ($\lambda_{eff} = 4$ as compared to 1). For instance, with 0.3 M (bi)carbonates, the degradation rate at $\lambda_{eff} = 4$ is two orders of magnitude slower compared to that at $\lambda_{eff} = 1$ (1.35×10^{-2} *versus* 6.35×10^{-4}, Table 1). This is also consistent with our previous work, which indicates that the degradation rate of $BTMA^+$ decreases with increasing hydration level.[28] However, it is noteworthy that the effect of (bi)carbonate remains prominent even when utilizing a higher hydration level ($\lambda_{eff} = 4$).

These results clearly show that the introduction of (bi) carbonate plays a crucial role in stabilizing the $BTMA^+$ cations.

However, the nominal concentration of hydroxide anions decreases as well while adding (bi)carbonates in the solutions. This raises the possibility that the reduced degradation could be attributed to the diminished presence of hydroxide in the system. To gain deeper insight into this phenomenon, we designed and conducted a new series of experiments wherein the hydroxide concentration was maintained constant while systematically varying only the concentration of (bi)carbonates.

Fig. 3 illustrates the changes in $BTMA^+$ remaining concentration during stability tests, where all experiments included the same hydroxide concentration of 0.7 M (NMR spectra in Fig. S15–S20, while Tables S17 and S18 contain the relevant data). Different concentrations of (bi)carbonates (0, 0.15, and 0.3 M) were added to the solutions. The experiments depicted in Fig. 3 were performed at 45 °C in DMSO-d_6 solutions, resulting in calculated λ_{OH^-} values of 1.4 and 5.7, respectively. Table 2 summarizes the degradation rates and the calculated $BTMA^+$ half-lives for all the experiments in Fig. 3. According to Fig. 3a ($\lambda_{OH^-} = 1.4$), the calculated half-lives are 17.2, 31.8, and 59.8 h corresponding to 0, 0.15, and 0.3 M (bi)carbonates, respectively. Thus, $BTMA^+$ degradation is slowed down by the addition of (bi) carbonates, even while the concentration of hydroxide is constant. The results depicted in Fig. 2b, considering a $\lambda_{OH^-} = 5.7$, exhibit a similar trend. In this case, the calculated half-lives for $BTMA^+$ degradation at 0, 0.15, and 0.3 M (bi)carbonates are 723, 1286, and 1438 h, respectively. Remarkably, when $\lambda_{OH^-} = 1.4$, the degradation rate is approximately 3.5 times slower in the presence of 0.3 M (bi)carbonates compared to their absence. Likewise, for $\lambda_{OH^-} = 5.7$, the degradation rate is approximately 2 times slower in the presence of bicarbonates. Hence, these findings suggest that not only does the addition of only 0.3 M (bi)carbonate to the medium result in a substantial decrease in the degradation rate of the $BTMA^+$, but also, the effect of CO_2 is more pronounced at lower hydration levels.

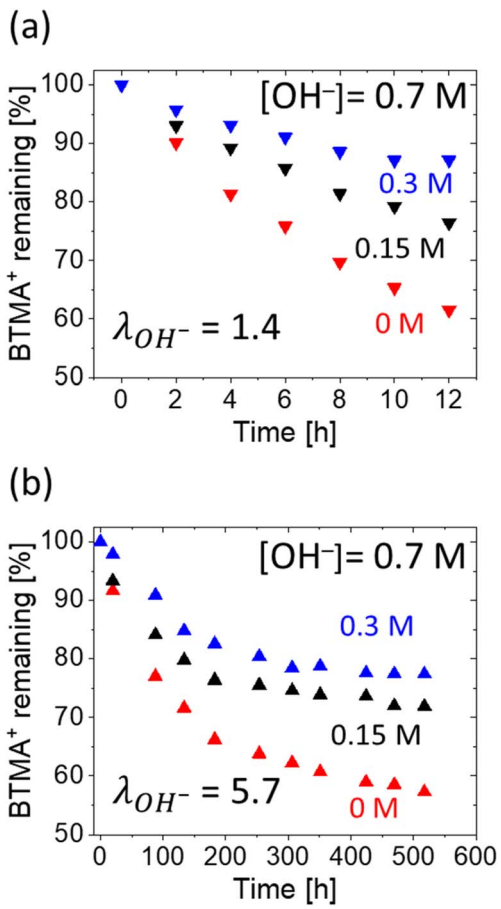

Fig. 3 Relative $BTMA^+$ remaining as a function of time in DMSO-d_6 solutions at 45 °C. All experiments initiate with an OH^-concentration of 0.7 M, while initial (bi)carbonate 0, 0.15, and 0.3 M (bi)carbonates for (a) $\lambda_{OH^-} = 1.4$, and (b) $\lambda_{OH^-} = 5.7$.

To investigate the impact of even lower concentration (bi) carbonates (0, 0.05 and 1 M) on $BTMA^+$ stability, additional stability tests were conducted using a higher hydroxide concentration of 0.9 M (NMR spectra are available in Fig. S21–S38, and the associated data can be found in Tables S19 and S20). The presence of (bi)carbonates undeniably contributed to the stabilization of $BTMA^+$, even when present at a lower concentration of (bi)carbonates.

The experimental results obtained in this study agree with previous MD research, which demonstrated that the presence of carbonate anions stabilizes the $BTMA^+$.[85] However, the question of whether the enhanced hydration of carbonate anions diminishes the hydration of hydroxide, thereby increasing nucleophilicity and subsequently degrading $BTMA^+$, remains unanswered.[85] Additionally, density functional theory (DFT) calculations report that the free energies of hydration for hydroxide and carbonate anions are −449 and −1213 kJ mol^{-1}, respectively.[96] Consequently, the introduction of bicarbonate should induce dehydration of hydroxide, potentially accelerating the degradation rate of $BTMA^+$.[28] This contradicts the experimental findings in this study but aligns with the previous MD study.[85]

A plausible explanation is that bicarbonate consumes hydroxide to form carbonate (eqn (2)). However, even if this were the case and we take the addition of 0.3 M bicarbonate to 0.7 M hydroxide as an example, the rate should be less than twice as slow. But in this study, the observed rate is 3.5 times slower, indicating that such a reaction leading to hydroxide concentration reductions cannot fully explain the change in rate. If this reaction is indeed complete, we are also introducing an additional 0.3 M of water, which in this hypothetical case would raise the overall λ_{eff} by 0.5.

To further study this rate reduction, we performed new MD simulations to further explore the effects of microsolvation of the different anions. Mixtures containing $BTMA^+$, hydroxide, and carbonate anions were simulated. Bromide anions were added as counterions to $BTMA^+$ and potassium cations were added to achieve overall charge balance. DMSO was used as an explicit solvent. Carbonate anions were chosen as opposed to bicarbonate anions because, at practical AEMFC current densities, the dominant species in the AEM during fuel cell operation are only hydroxide and carbonate anions.[76] Moreover, carbonate provides a "worst case scenario" as it is more hygroscopic than bicarbonate.[96]

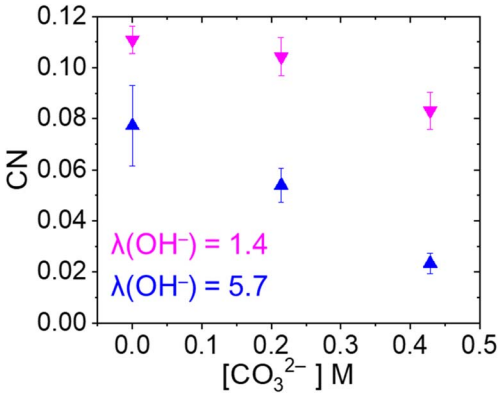

Fig. 4 Average coordination number (CN) of OH^- anions around $BTMA^+$ as a function of carbonate concentrations for solutions of 0.7 M OH^- and $\lambda(OH^-) = 1.4$ and 5.7.

Fig. 4 presents the coordination number (CN) of OH^- anions around $BTMA^+$ in a solution containing 0.7 M OH^- and with varying carbonate concentrations (0, 0.15, and 0.3 M) for $\lambda(OH^-) = 1.4$ and 5.7. Without carbonates, there is an average of 0.11 and 0.08 OH^- anions surrounding $BTMA^+$ at $\lambda(OH^-) = 1.4$ and 5.7, respectively. In other words, $BTMA^+$ interacts with an OH^- anion around 11% and 8% of the time, respectively. With 0.15 M carbonates, these values decrease to 10% and 5%. At 0.3 M carbonates, only 8% and 2% of $BTMA^+$ are surrounded by OH^- at $\lambda(OH^-) = 1.4$ and 5.7, respectively. Thus, for both $\lambda(OH^-) = 1.4$ and 5.7, the introduction of 0.15 and 0.3 M carbonate anions results in a decrease of at least 10% and 70% in the CNs, respectively, compared to scenarios where no carbonate is present, highlighting the significant impact of adding carbonate to the system. Notably, the CNs at higher $\lambda(OH^-)$ are smaller. This is due to the greater hydration of the hydroxides at higher $\lambda(OH^-)$, as is further discussed below.

The MD simulations validate that the addition of more carbonates reduces the CNs of OH^- anions surrounding $BTMA^+$. This effectively stabilizes the $BTMA^+$. These results align with the experimental data depicted in Fig. 3 of this study, illustrating that the presence of carbonates serves as a stabilizer for $BTMA^+$. Also, this effect is particularly pronounced under conditions of low hydration levels. Consequently, the subsequent objective was to investigate the causes of this "stabilizer" phenomenon.

Inspection and analysis of the snapshots from the MD simulations (Fig. 5) indicate that the addition of carbonate anions drives the system towards microphase segregations between an "aqueous phase", made of aqueous microbubbles encompassing the water molecules, hydroxide, carbonate anions and counterions (not shown); and an "organic domain" which comprises the DMSO and $BTMA^+$ molecules. Fig. 5 shows the largest aqueous cluster, composed only of water molecules and ionic species, that is phase-separated from the DMSO solvent (DMSO is not shown for clarity). Although DMSO is not present in real cells, it was used as a solvent to enable *ex situ* investigation of degradation under very low hydration. As shown in our earlier work,[28] this approach mimics real cell

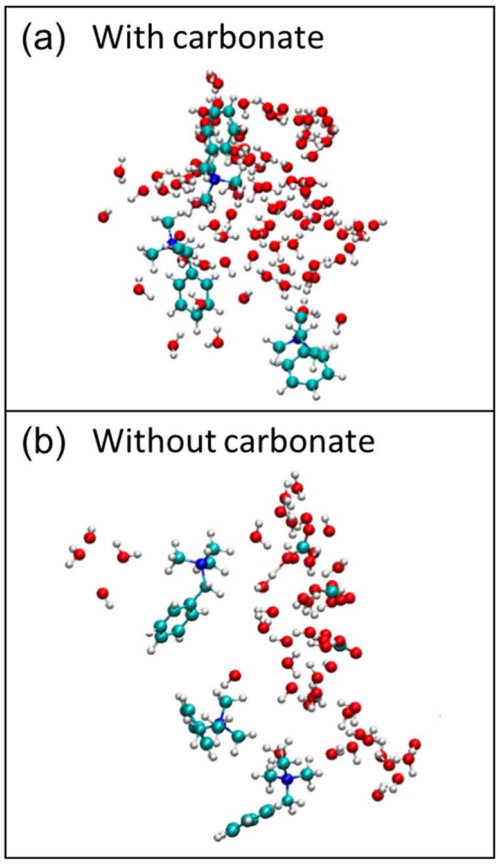

Fig. 5 MD-derived configurations at $\lambda(OH^-)$=5.7 illustrate the water phase under two conditions: in the presence (a) and absence (b) of carbonate. The aqueous phase is easily distinguished and contains water, hydroxide, and carbonate molecules (only in a), while the larger $BTMA^+$ molecules can be seen surrounding the aqueous phase with the charged end at the interface. H in white, C in cyan, N in blue, O in red. DMSO, Br^-, and K^+ omitted for clarity.

conditions where water depletion at the cathode increases OH^- nucleophilicity, accelerating cation degradation. The DMSO system reproduces this regime in a controlled manner, complementing in-cell observations. Fig. 5 also shows that $BTMA^+$ molecules are located at the interface between the two phases. This is similar to the well-known "salting-out" effect used in organic chemistry, in which increasing the ionic strength leads to better and faster phase separation.[97,98] Inside the aqueous domain, the carbonate effectively reduces the hydroxide microsolvation as it binds water more strongly, as indicated by DFT.[96] However, this hydroxide is still part of the aqueous phase but has a lower probability of reaching the interface and attacking $BTMA^+$.

Fig. 6 shows the average number of water (blue) and free OH^- (pink) molecules in the aqueous cluster when carbonate is present or absent for both cases of $\lambda(OH^-) = 1.4$ and 5.7. As suggested, the addition of carbonate leads to larger aqueous clusters. For instance, the average number of water molecules in clusters rises from 55.41 to 84.55 when carbonate anions are introduced into the system at $\lambda(OH^-) = 1.4$, and from 38.63 to 50.42 at $\lambda(OH^-) = 5.7$. On the other hand, the average number

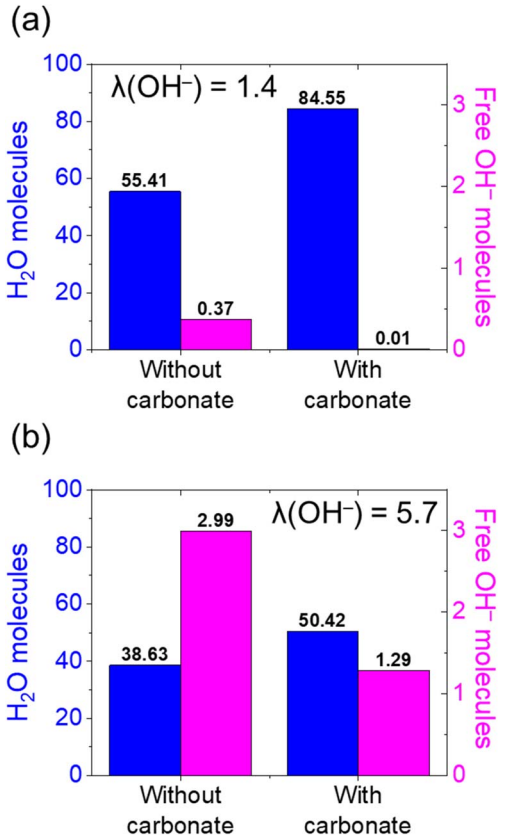

Fig. 6 The average number of water molecules in aqueous cluster and the average number of free OH^- anions with and without carbonates for (a) $\lambda(OH^-) = 1.4$ and (b) 5.7.

of free hydroxide anions in the cluster decreases with the additions of carbonate (from 0.37 to 0.01 for $\lambda(OH^-) = 1.4$, and from 2.99 to 1.29 for $\lambda(OH^-) = 5.7$).

The results in Fig. 6 further support the "salting out" effect, demonstrating that the addition of carbonate increases the size of the aqueous cluster due to this phenomenon. Moreover, the decrease in the number of free hydroxide ions is attributed to their involvement in reactions (eqn (1) and (2)) to form carbonate and water species. This effect is most pronounced at low hydration, aligning with the experimental results and highlighting the stabilizing role of carbonate anions on AEM cationic groups.

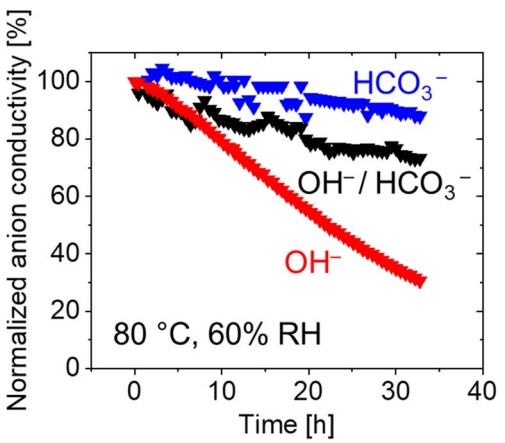

Fig. 7 Normalized anion conductivity of AEMs as a function of time at 80 °C, 60% RH, and 500 standard cubic centimeters (sccm) min^{-1} N_2 gas.

To provide additional support for the fact that the presence of CO_2 anions reduces AEM degradation, we developed a new protocol to test the alkaline stability of membranes *ex situ*. The test measures the anion conductivity decay during the degradation test time while controlling the levels of bicarbonate anions present in the AEM. This new protocol also advances our abilities towards more representative stability tests and data for electrochemical devices and better simulates AEMFC and AEMWE environments. The anion conductivity was measured in AEMs in three different ionic forms: OH^- form, HCO_3^- form, and in a OH^-/HCO_3^- mixed form. Detailed information regarding this new protocol can be found in the experimental section. Throughout all the conducted experiments, the degradation of the AEMs was measured by the decay in their anion conductivity over time.

Fig. 7 illustrates the decay of normalized anion conductivity of AEMs in their different forms (OH^-, HCO_3^-, and OH^-/HCO_3^- mixed form) as a function of time using a nitrogen environment set at 60% RH at 80 °C. The combination of high temperature and very low RH induces a low hydration level in the AEMs, and therefore, fast degradation kinetics.[67] As can be seen in Fig. 7, the AEM exhibited the highest stability when it is in its HCO_3^- form, reaching *ca.* 88% anion conductivity retention after 33 h. However, the AEM in its OH^- form displayed lower stability, retaining only *ca.* 31% of anion conductivity after 33 h. Moreover, the result obtained in the OH^-/HCO_3^- mixed form test shows that the AEM degrades much slower than OH^- form, with a slope closer to the HCO_3^- one. The AEM in both HCO_3^- and OH^-/HCO_3^- mixed forms exhibited relatively high alkali stability, with a measured conductivity decay value of only 0.5 and 0.7% h^{-1}, respectively. In contrast, the AEM in the hydroxide form displayed a higher conductivity decay value of 2.3% h^{-1}. The decay of normalized anion conductivities followed a generally linear trend, indicating that the degradation rates of conductivity remained relatively constant throughout the stability test. These findings, as depicted in Fig. 7, provide further evidence that an AEM in its bicarbonate form exhibits slower degradation under low RH conditions, while the OH^- form experiences significantly faster degradation.

4. Conclusions

AEMFC development is hindered by operating challenges in ambient air, mainly due to CO_2 causing rapid carbonation and reducing cell performance. Furthermore, the impact of CO_2 on AEMWE fed with water hasn't been studied yet. In this work, we studied for the first time the effect of the presence of (bi) carbonates on the chemical stability of $BTMA^+$ cations. The experiments were performed with different OH^-: HCO_3^- ratios, as well as with the same OH^- concentration and different

HCO_3^- concentrations. Results indicate that inducing CO_2 reduces the degradation rates and therefore improves the chemical stability of the $BTMA^+$ cations. In addition, similar to pure hydroxide systems, as hydration levels decrease, the degradation rates are accelerated, yet the carbonation stabilizer effect is stronger at lower hydration levels. These experimental results are supported by MD simulations that show that OH^- coordination around $BTMA^+$ is higher at lower hydration, but decreases substantially with carbonation, particularly at very low hydration levels. Based on our MD findings, we propose that the stability of $BTMA^+$ in the presence of carbonate anions may be due to the "salting-out" effect, particularly pronounced at lower hydration levels. Although exposing an AEMFC cell to CO_2 causes a moderate reduction in the anion conductivity, our results suggest that running cells in contact with CO_2 may inhibit membrane degradation and increase the operating lifetimes. This stabilization effect in AEM may also be attributed to the "salting-out" phenomenon, similar to that observed with $BTMA^+$. Consequently, the potential utilization of AEM with (bi) carbonate anions in electrochemical devices for prolonged durations necessitated further investigation. We strongly believe that these findings will promote the development of highly stable AEMs for electrochemical applications.

Author contributions

Sapir Willdorf-Cohen: investigation, methodology, formal analysis, writing – original draft. Songlin Li: formal analysis. Simcha Srebnik: formal analysis, writing – review & editing. Charles E. Diesendruck: conceptualization, writing – review & editing, supervision, resources, funding acquisition, project administration. Dario R. Dekel: conceptualization, writing – review & editing, supervision, resources, funding acquisition, project administration.

Conflicts of interest

The authors declare no conflict of interest.

Data availability

The data supporting this article are provided in the SI, and additional raw data are available from the corresponding authors upon reasonable request. The SI includes representative calculations, degradation rates with calculated half-lives, and ^{1}H-NMR spectra for the degradation kinetics of $BTMA^+$ under different conditions as described in the manuscript. See DOI: **https://doi.org/10.1039/d5ta06137g**.

Acknowledgements

This work was partially funded by the Nancy & Stephen Grand Technion Energy Program (GTEP); by the Israel National Institute for Energy Storage (INIES); by the Ministry of National Infrastructure, Energy and Water Resources of Israel through grant No. 3-17591 (220-11-040); by the Israeli Science Foundation (ISF) grant number 169/22; by the European Union's Horizon 2021 research and innovation program, under grant agreement 101071111; by the European Union's Horizon 2024 research and innovation program under grant agreement 101192454; by the National Authority for Technological Innovation through grant No. 2034042; and by the council for higher education, Flagship Initiatives and Applied Research Strategy and International Affairs Division on Sustainability and the Climate Crisis, grant No. 2072133.

References

1 M. Faour, K. Yassin and D. R. Dekel, Anion-Exchange Membrane Oxygen Separator, *ACS Org. Inorg. Au*, 2024, **4, 5**, 498–503.
2 D. Li, E. J. Park, W. Zhu, Q. Shi, Y. Zhou, H. Tian, *et al.*, Highly quaternized polystyrene ionomers for high performance anion exchange membrane water electrolysers, *Nat. Energy*, 2020, **5**(5), 378–385.
3 M. Chatenet, B. G. Pollet, D. R. Dekel, F. Dionigi, J. Deseure, P. Millet, *et al.*, Water electrolysis: from textbook knowledge to the latest scientific strategies and industrial developments, *Chem. Soc. Rev.*, 2022, **51**(11), 4583–4762.
4 N. Zion, J. C. Douglin, D. A. Cullen, P. Zelenay, D. R. Dekel and L. Elbaz, Porphyrin Aerogel Catalysts for Oxygen Reduction Reaction in Anion-Exchange Membrane Fuel Cells, *Adv. Funct. Mater.*, 2021, **31**(24), 1–7.
5 Y. Xue, L. Shi, X. Liu, J. Fang, X. Wang, B. P. Setzler, *et al.*, A highly-active, stable and low-cost platinum-free anode catalyst based on RuNi for hydroxide exchange membrane fuel cells, *Nat. Commun.*, 2020, **11**(1), 1–8.
6 X. Peng, T. J. Omasta, E. Magliocca, L. Wang, J. R. Varcoe and W. E. Mustain, Nitrogen-doped Carbon–CoO x Nanohybrids: A Precious Metal Free Cathode that Exceeds 1.0 W cm^{-2} Peak Power and 100 h Life in Anion-Exchange Membrane Fuel Cells, *Angew. Chem.*, 2019, **131**(4), 1058–1063.
7 T. Huang, H. Jiang, J. C. Douglin, Y. Chen, S. Yin, J. Zhang, *et al.*, Single Solution-Phase Synthesis of Charged Covalent Organic Framework Nanosheets with High Volume Yield. Angew. Chem., Int. Ed., 2023, **62**(4), e202209306. available from: **https://onlinelibrary.wiley.com/doi/10.1002/anie.202209306**.
8 Z. S. Campagna, M. L. Faro, A. Carbone, C. Italiano, S. Trocino, G. Monforte, *et al.*, Performance and stability of a critical raw materials-free anion exchange membrane electrolysis cell, *Electrochim. Acta*, 2022, **413**, 140078.
9 Y. C. Cao, X. Wu and K. Scott, A quaternary ammonium grafted poly vinyl benzyl chloride membrane for alkaline anion exchange membrane water electrolysers with non-noble-metal catalysts, *Int. J. Hydrogen Energy*, 2012, **37**(12), 9524–9528.
10 P. G. Santori, F. D. Speck, S. Cherevko, H. A. Firouzjaie, X. Peng, W. E. Mustain, *et al.*, High Performance FeNC and Mn-oxide/FeNC Layers for AEMFC Cathodes, *J. Electrochem. Soc.*, 2020, **167**(13), 134505.
11 J. Biemolt, J. C. Douglin, R. K. Singh, E. S. Davydova, N. Yan, G. Rothenberg, *et al.*, An Anion-Exchange Membrane Fuel

Cell Containing Only Abundant and Affordable Materials, *Energy Technol.*, 2021, **9**(4), 5–9.
12 D. R. Dekel, Alkaline Membrane Fuel Cell (AMFC) Materials and System Improvement – State-of-the-Art, *ECS Trans.*, 2013, **50**(2), 2051–2052.
13 N. Ziv, A. N. Mondal, T. Weissbach, S. Holdcroft and D. R. Dekel, Effect of CO_2 on the properties of anion exchange membranes for fuel cell applications, *J. Membr. Sci.*, 2019, **586**, 140–150.
14 Y. Zheng, L. N. I. Colón, N. U. Hassan, E. R. Williams, M. Stefik, J. M. Lamanna, *et al.*, Effect of membrane properties on the carbonation of anion exchange membrane fuel cells, *Membranes*, 2021, **11**(2), 1–14.
15 M. R. Sturgeon, C. S. Macomber, C. Engtrakul, H. Long and B. S. Pivovar, Hydroxide based Benzyltrimethylammonium Degradation: Quantification of Rates and Degradation Technique Development, *J. Electrochem. Soc.*, 2015, **162**(4), F366–F372.
16 B. Chen, P. Mardle and S. Holdcroft, Probing the effect of ionomer swelling on the stability of anion exchange membrane water electrolyzers, *J. Power Sources*, 2022, **550**, 232134.
17 M. Liu, X. Hu, B. Hu, L. Liu and N. Li, Soluble poly(aryl piperidinium) with extended aromatic segments as anion exchange membranes for alkaline fuel cells and water electrolysis, *J. Membr. Sci.*, 2022, **642**, 119966.
18 N. Du, C. Roy, R. Peach, M. Turnbull, S. Thiele and C. Bock, Anion-Exchange Membrane Water Electrolyzers, *Chem. Rev.*, 2022, **122**(13), 11830–11895.
19 A. D. Mohanty and C. Bae, Mechanistic analysis of ammonium cation stability for alkaline exchange membrane fuel cells, *J. Mater. Chem. A*, 2014, **2**(41), 17314–17320.
20 A. D. Mohanty, S. E. Tignor, M. R. Sturgeon, H. Long, B. S. Pivovar and C. Bae, Thermochemical Stability Study of Alkyl-Tethered Quaternary Ammonium Cations for Anion Exchange Membrane Fuel Cells, *J. Electrochem. Soc.*, 2017, **164**(13), F1279–F1285.
21 D. Pan, J. S. Olsson and P. Jannasch, Poly(fluorene alkylene) Anion Exchange Membranes with Pendant Spirocyclic and Bis-Spirocyclic Quaternary Ammonium Cations, *ACS Appl. Energy Mater.*, 2022, **5**(1), 981–991.
22 Q. Wei, X. Cao, P. Veh, A. Konovalova, P. Mardle, P. Overton, *et al.*, On the stability of anion exchange membrane fuel cells incorporating polyimidazolium ionene (Aemion+®) membranes and ionomers, *Sustainable Energy Fuels*, 2022, **6**(15), 3551–3564.
23 J. Xue, J. Zhang, X. Liu, T. Huang, H. Jiang, Y. Yin, *et al.*, Toward alkaline-stable anion exchange membranes in fuel cells: cycloaliphatic quaternary ammonium-based anion conductors, *Electrochem. Energy Rev.*, 2022, **5**(2), 348–400.
24 L. Yin, R. Ren, L. He, W. Zheng, Y. Guo, L. Wang, *et al.*, Stable Anion Exchange Membrane Bearing Quinuclidinium for High-performance Water Electrolysis, *Angew. Chem., Int. Ed.*, 2024, 202400764.
25 R. Wang, M. Ohashi, M. Ishida and H. Ito, Water transport analysis during cathode dry operation of anion exchange membrane water electrolysis, *Int. J. Hydrogen Energy*, 2022, **47**(97), 40835–40848.
26 C. E. Diesendruck and D. R. Dekel, Water – A key parameter in the stability of anion exchange membrane fuel cells, *Curr. Opin. Electrochem.*, 2018, **9**, 173–178.
27 J. Fan, S. Willdorf-Cohen, E. M. Schibli, Z. Paula, W. Li, T. J. G. Skalski, *et al.*, Poly(bis-arylimidazoliums) possessing high hydroxide ion exchange capacity and high alkaline stability, *Nat. Commun.*, 2019, **10**(1), 2306.
28 D. R. Dekel, M. Amar, S. Willdorf, M. Kosa, S. Dhara and C. E. Diesendruck, Effect of Water on the Stability of Quaternary Ammonium Groups for Anion Exchange Membrane Fuel Cell Applications, *Chem. Mater.*, 2017, **29**(10), 4425–4431.
29 D. R. Dekel, S. Willdorf, U. Ash, M. Amar, S. Pusara, S. Dhara, *et al.*, The critical relation between chemical stability of cations and water in anion exchange membrane fuel cells environment, *J. Power Sources*, 2018, **375**, 351–360.
30 I. Zadok, H. Long, B. Pivovar, A. Roznowska, A. Michalak, D. R. Dekel, *et al.*, Unexpected hydroxide ion structure and properties at low hydration, *J. Mol. Liq.*, 2020, **313**, 113485.
31 S. Willdorf-Cohen, A. Kaushansky, D. R. Dekel and C. E. Diesendruck, Hydroxide Chemoselectivity Changes with Water Microsolvation, *J. Phys. Chem. Lett.*, 2022, **13**(43), 10216–10221.
32 D. R. Dekel, I. G. Rasin, M. Page and S. Brandon, Steady state and transient simulation of anion exchange membrane fuel cells, *J. Power Sources*, 2018, **375**, 191–204.
33 C. L. Radford, T. Saatkamp, A. J. Bennet and S. Holdcroft, An organic proton cage that is ultra-resistant to hydroxide-promoted degradation, *Nat. Commun.*, 2024, **15**(1), 1–7.
34 D. R. Dekel, I. G. Rasin and S. Brandon, Predicting performance stability of anion exchange membrane fuel cells, *J. Power Sources*, 2019, **420**, 118–123.
35 K. Yassin, I. G. Rasin, S. Brandon and D. R. Dekel, Quantifying the critical effect of water diffusivity in anion exchange membranes for fuel cell applications, *J. Membr. Sci.*, 2020, **608**, 118206.
36 G. Gupta, K. Scott and M. Mamlouk, Soluble Polystyrene-*b*-poly (ethylene/butylene)-*b*-polystyrene Based Ionomer for Anion Exchange Membrane Fuel Cells Operating at 70 °C, *Fuel Cells*, 2018, **18**(2), 137–147.
37 P. Veh, B. Britton, S. Holdcroft, R. Zengerle, S. Vierrath and M. Breitwieser, Improving the water management in anion-exchange membrane fuel cells: *via* ultra-thin, directly deposited solid polymer electrolyte, *RSC Adv.*, 2020, **10**(15), 8645–8652.
38 M. G. Marino and K. D. Kreuer, Alkaline Stability of Quaternary Ammonium Cations for Alkaline Fuel Cell Membranes and Ionic Liquids, *ChemSusChem*, 2015, **8**(3), 513–523.
39 L. Wang, M. Bellini, H. A. Miller and J. R. Varcoe, A high conductivity ultrathin anion-exchange membrane with 500+ h alkali stability for use in alkaline membrane fuel cells that can achieve 2 W cm-2 at 80 °C, *J. Mater. Chem. A*, 2018, **6**(31), 15404–15412.
40 L. Wang, X. Peng, W. E. Mustain and J. R. Varcoe, Radiation-grafted anion-exchange membranes: The switch from low- to

high-density polyethylene leads to remarkably enhanced fuel cell performance, *Energy Environ. Sci.*, 2019, **12**(5), 1575–1579.
41 S. Noh, J. Y. Jeon, S. Adhikari, Y. S. Kim and C. Bae, Molecular Engineering of Hydroxide Conducting Polymers for Anion Exchange Membranes in Electrochemical Energy Conversion Technology, *Acc. Chem. Res.*, 2019, **52**(9), 2745–2755.
42 L. Gu, H. Dong, Z. Sun, Y. Li and F. Yan, Spirocyclic quaternary ammonium cations for alkaline anion exchange membrane applications: an experimental and theoretical study, *RSC Adv.*, 2016, **6**(97), 94387–94398.
43 J. S. Olsson, T. H. Pham and P. Jannasch, Poly(*N*,*N*-diallylazacycloalkane)s for Anion-Exchange Membranes Functionalized with N-Spirocyclic Quaternary Ammonium Cations, *Macromolecules*, 2017, **50**(7), 2784–2793.
44 Z. Sun, B. Lin and F. Yan, Anion-Exchange Membranes for Alkaline Fuel-Cell Applications: The Effects of Cations, *ChemSusChem*, 2018, **11**(1), 58–70.
45 W. You, K. J. T. Noonan and G. W. Coates, Alkaline-stable anion exchange membranes: a review of synthetic approaches, *Prog. Polym. Sci.*, 2020, **100**, 101177.
46 Z. Tao, C. Wang, X. Zhao, J. Li and M. D. Guiver, Progress in High-Performance Anion Exchange Membranes Based on the Design of Stable Cations for Alkaline Fuel Cells, *Adv. Mater. Technol.*, 2021, **6**(5), 1–14.
47 S. Adhikari, M. K. Pagels, J. Y. Jeon and C. Bae, Ionomers for electrochemical energy conversion & storage technologies, *Polymer*, 2020, **211**, 123080.
48 Q. Wei, X. Cao, P. Veh, A. Konovalova, P. Mardle, P. Overton, *et al.*, On the stability of anion exchange membrane fuel cells incorporating polyimidazolium ionene (Aemion+®) membranes and ionomers, *Sustainable Energy Fuels*, 2022, **6**(15), 3551–3564.
49 N. Gjineci, S. Aharonovich, D. R. Dekel and C. E. Diesendruck, Increasing the Alkaline Stability of *N*,*N*-Diaryl Carbazolium Salts Using Substituent Electronic Effects, *ACS Appl. Mater. Interfaces*, 2020, **12**(44), 49617–49625.
50 M. S. Cha, J. E. Park, S. Kim, S. H. Han, S. H. Shin, S. H. Yang, *et al.*, Poly(carbazole)-based anion-conducting materials with high performance and durability for energy conversion devices, *Energy Environ. Sci.*, 2020, **13**(10), 3633–3645.
51 D. Liu, L. Lin, Y. Xie, J. Pang and Z. Jiang, Anion exchange membrane based on poly(arylene ether ketone) containing long alkyl densely quaternized carbazole derivative pendant, *J. Membr. Sci.*, 2021, **623**, 119079.
52 K. Aggarwal, N. Gjineci, A. Kaushansky, S. Bsoul, J. C. Douglin, S. Li, *et al.*, Isoindolinium Groups as Stable Anion Conductors for Anion-Exchange Membrane Fuel Cells and Electrolyzers, *ACS Mater. Au*, 2022, **2**(3), 367–373.
53 Q. Wang, L. Huang, J. Zheng, Q. Zhang, G. Qin, S. Li, *et al.*, Design, synthesis and characterization of anion exchange membranes containing guanidinium salts with ultrahigh dimensional stability, *J. Membr. Sci.*, 2022, **643**(2021), 120008.
54 L. Liu, Q. Li, J. Dai, H. Wang, B. Jin and R. Bai, A facile strategy for the synthesis of guanidinium-functionalized polymer as alkaline anion exchange membrane with improved alkaline stability, *J. Membr. Sci.*, 2014, **453**, 52–60.
55 F. P. Tipp, K. Fraser, M. J. Eslamibidgoli, K. Malek, S. Holdcroft and M. H. Eikerling, Stability Descriptors for (Benz)imidazolium-Based Anion Exchange Membranes, *Macromolecules*, 2024, **57**(4), 1734–1743.
56 M. A. Hossain, H. Jang, S. C. Sutradhar, J. Ha, J. Yoo, C. Lee, *et al.*, Novel hydroxide conducting sulfonium-based anion exchange membrane for alkaline fuel cell applications, *Int. J. Hydrogen Energy*, 2016, **41**(24), 10458–10465.
57 K. J. T. Noonan, K. M. Hugar, H. a Kostalik, E. B. Lobkovsky, H. D. Abruña and G. W. Coates, Phosphonium-Functionalized Polyethylene: A New Class of Base-Stable Alkaline Anion Exchange Membranes, *J. Am. Chem. Soc.*, 2012, **134**(44), 18161–18164.
58 M. Kumari, J. C. Douglin and D. R. Dekel, Crosslinked quaternary phosphonium-functionalized poly(ether ether ketone) polymer-based anion-exchange membranes, *J. Membr. Sci.*, 2021, **626**, 119167.
59 S. Miyanishi and T. Yamaguchi, Ether cleavage-triggered degradation of benzyl alkylammonium cations for polyethersulfone anion exchange membranes, *Phys. Chem. Chem. Phys.*, 2016, **18**, 12009–12023.
60 X. Liu, N. Xie, J. Xue, M. Li, C. Zheng, J. Zhang, *et al.*, Magnetic-field-oriented mixed-valence-stabilized ferrocenium anion-exchange membranes for fuel cells, *Nat. Energy*, 2022, **7**(4), 329–339.
61 K. Aggarwal, S. Bsoul, S. Li, D. R. Dekel and C. E. Diesendruck, Ligand Valency Effects on the Alkaline Stability of Metallopolymer Anion-Exchange Membranes, *Macromol. Rapid Commun.*, 2021, **42**(16), 2100238.
62 M. L. Disabb-Miller, Y. Zha, A. J. DeCarlo, M. Pawar, G. N. Tew and M. a Hickner, Water Uptake and Ion Mobility in Cross-Linked Bis(terpyridine)ruthenium-Based Anion Exchange Membranes, *Macromolecules*, 2013, **46**(23), 9279–9287.
63 T. Zhu, Y. Sha, H. A. Firouzjaie, X. Peng, Y. Cha, D. M. M. M. Dissanayake, *et al.*, Rational Synthesis of Metallo-Cations Toward Redox- And Alkaline-Stable Metallo-Polyelectrolytes, *J. Am. Chem. Soc.*, 2020, **142**(2), 1083–1089.
64 K. Aggarwal, S. Li, S. Nijem, D. R. Dekel and C. E. Diesendruck, Polymer Backbone Chemistry Shapes the Alkaline Stability of Metallopolymer Anion-Exchange Membranes, *Chem.—Eur. J.*, 2024, **30**(20), 1–5.
65 M. T. Kwasny, L. Zhu, M. A. Hickner and G. N. Tew, Utilizing thiol–ene chemistry for crosslinked nickel cation-based anion exchange membranes, *J. Polym. Sci., Part A: Polym. Chem.*, 2018, **56**(3), 328–339.
66 S. Haj-Bsoul, J. R. Varcoe and D. R. Dekel, Measuring the alkaline stability of anion-exchange membranes, *J. Electroanal. Chem.*, 2022, **908**, 116112.
67 J. Müller, A. Zhegur, U. Krewer, J. R. Varcoe and D. R. Dekel, Practical *Ex Situ* Technique to Measure the Chemical Stability of Anion-Exchange Membranes under Conditions

Simulating the Fuel Cell Environment, *ACS Mater. Lett.*, 2020, **2**(2), 168–173.

68 K. D. Kreuer and P. Jannasch, A practical method for measuring the ion exchange capacity decrease of hydroxide exchange membranes during intrinsic degradation, *J. Power Sources*, 2018, **375**, 361–366.

69 S. Willdorf-Cohen, A. N. Mondal, D. R. Dekel and C. E. Diesendruck, Chemical stability of poly(phenylene oxide)-based ionomers in an anion exchange-membrane fuel cell environment, *J. Mater. Chem. A*, 2018, **6**(44), 22234–22239.

70 S. Willdorf-Cohen, A. Zhegur-Khais, J. Ponce-González, S. Bsoul-Haj, J. R. Varcoe, C. E. Diesendruck, *et al.*, Alkaline Stability of Anion-Exchange Membranes, *ACS Appl. Energy Mater.*, 2023, **6**(2), 1085–1092.

71 Z. Si, L. Qiu, H. Dong, F. Gu, Y. Li and F. Yan, Effects of Substituents and Substitution Positions on Alkaline Stability of Imidazolium Cations and Their Corresponding Anion-Exchange Membranes, *ACS Appl. Mater. Interfaces*, 2014, **6**(6), 4346–4355.

72 S. Koch, J. Disch, S. K. Kilian, Y. Han, L. Metzler, A. Tengattini, *et al.*, Water management in anion-exchange membrane water electrolyzers under dry cathode operation, *RSC Adv.*, 2022, **12**(32), 20778–20784.

73 A. M. Oliveira, B. P. Setzler and Y. Yan, Study of pH Gradients and Carbonation of Hydroxide Exchange Membrane Electrolyzers, *J. Electrochem. Soc.*, 2025, **172**(2), 024509.

74 S. A. Lee, J. Kim, K. C. Kwon, S. H. Park and H. W. Jang, Anion exchange membrane water electrolysis for sustainable large-scale hydrogen production, *Carbon Neutralization*, 2022, **1**(1), 26–48.

75 M. Mandal, Recent Advancement on Anion Exchange Membranes for Fuel Cell and Water Electrolysis, *Chemelectrochem*, 2021, **8**(1), 36–45.

76 U. Krewer, C. Weinzierl, N. Ziv and D. R. Dekel, Impact of carbonation processes in anion exchange membrane fuel cells, *Electrochim. Acta*, 2018, **263**, 433–446.

77 N. Ziv, W. E. Mustain and D. R. Dekel, The Effect of Ambient Carbon Dioxide on Anion-Exchange Membrane Fuel Cells, *ChemSusChem*, 2018, **11**(7), 1136–1150.

78 D. Henkensmeier, M. Najibah, C. Harms, J. Zitka, J. Hnat and K. Bouzek, Overview: State-of-the Art Commercial Membranes for Anion Exchange Membrane Water Electrolysis, *J. Electrochem. Energy Convers. Storage*, 2021, **18**(2), 024001.

79 B. Chen, P. Mardle and S. Holdcroft, Probing the effect of ionomer swelling on the stability of anion exchange membrane water electrolyzers, *J. Power Sources*, 2022, **550**, 232134.

80 J. Li, C. Liu, J. Ge, W. Xing and J. Zhu, Challenges and Strategies of Anion Exchange Membranes in Hydrogen-electricity Energy Conversion Devices, *Chem.—Eur. J.*, 2023, **29**(26), e202203173.

81 Y. Zheng, G. Huang, M. Mandal, J. R. Varcoe, P. A. Kohl and W. E. Mustain, Editors' Choice—Power-Generating Electrochemical CO_2 Scrubbing from Air Enabling Practical AEMFC Application, *J. Electrochem. Soc.*, 2021, **168**(2), 024504.

82 Y. Zheng, T. J. Omasta, X. Peng, L. Wang, J. R. Varcoe, B. S. Pivovar, *et al.*, Quantifying and elucidating the effect of CO_2 on the thermodynamics, kinetics and charge transport of AEMFCs, *Energy Environ. Sci.*, 2019, **12**(9), 2806–2819.

83 M. R. Gerhardt, L. M. Pant and A. Z. Weber, Along-the-channel impacts of water management and carbon-dioxide contamination in hydroxide-exchange-membrane fuel cells: a modeling study, *J. Electrochem. Soc.*, 2019, **166**(7), F3180–F3192.

84 Y. Zheng, G. Huang, L. Wang, J. R. Varcoe, P. A. Kohl and W. E. Mustain, Effect of reacting gas flowrates and hydration on the carbonation of anion exchange membrane fuel cells in the presence of CO2, *J. Power Sources*, 2020, **467**(May), 228350.

85 S. Srebnik, S. Pusara and D. R. Dekel, Effect of Carbonate Anions on Quaternary Ammonium-Hydroxide Interaction, *J. Phys. Chem. C*, 2019, **123**(26), 15956–15962.

86 M. Krauβ and R. Rzehak, Reactive absorption of CO_2 in NaOH: detailed study of enhancement factor models, *Chem. Eng. Sci.*, 2017, **166**, 193–209.

87 N. Ziv and D. R. Dekel, A practical method for measuring the true hydroxide conductivity of anion exchange membranes, *Electrochem. Commun.*, 2018, **88**, 109–113.

88 A. Zhegur-Khais, F. Kubannek, U. Krewer and D. R. Dekel, Measuring the true hydroxide conductivity of anion exchange membranes, *J. Membr. Sci.*, 2020, **612**, 118461.

89 N. P. Kryuchkov, S. O. Yurchenko, Y. D. Fomin, E. N. Tsiok and V. N. Ryzhov, Complex crystalline structures in a two-dimensional core-softened system, *Soft Matter*, 2018, **14**(11), 2152–2162.

90 H. J. C. Berendsen, J. R. Grigera and T. P. Straatsma, The missing term in effective pair potentials, *J. Phys. Chem.*, 1987, **91**(24), 6269–6271.

91 A. D. MacKerell, D. Bashford, M. Bellott, R. L. Dunbrack, J. D. Evanseck, M. J. Field, *et al.*, All-atom empirical potential for molecular modeling and dynamics studies of proteins, *J. Phys. Chem. B*, 1998, **102**(18), 3586–3616.

92 W. L. Jorgensen, D. S. Maxwell and J. Tirado-Rives, Development and testing of the OPLS all-atom force field on conformational energetics and properties of organic liquids, *J. Am. Chem. Soc.*, 1996, **118**(45), 11225–11236.

93 M. P. Allen and D. J. Tildesley, *Computer Simulation of Liquids*. Oxford University Press, 2017.

94 R. Espiritu, B. T. Golding, K. Scott and M. Mamlouk, Degradation of radiation grafted hydroxide anion exchange membrane immersed in neutral pH: removal of vinylbenzyl trimethylammonium hydroxide due to oxidation, *J. Mater. Chem. A*, 2017, **5**(3), 1248–1267.

95 P. Mansouri Bakvand and P. Jannasch, Poly(arylene alkylene)s with pendent benzyl-tethered ammonium cations for anion exchange membranes, *J. Membr. Sci.*, 2023, **668**(2022), 121229.

96 M. P. Andersson and S. L. S. Stipp, Predicting hydration energies for multivalent ions, *J. Comput. Chem.*, 2014, **35**(28), 2070–2075.
97 A. M. Hyde, S. L. Zultanski, J. H. Waldman, Y. L. Zhong, M. Shevlin and F. Peng, General Principles and Strategies for Salting-Out Informed by the Hofmeister Series, *Org. Process Res. Dev.*, 2017, **21**(9), 1355–1370.
98 K. P. Gregory, G. R. Elliott, H. Robertson, A. Kumar, E. J. Wanless, G. B. Webber, *et al.*, Understanding specific ion effects and the Hofmeister series, *Phys. Chem. Chem. Phys.*, 2022, **24**(21), 12682–12718.

